Eur. Phys. J. C (2023) 83:186
https://doi.org/10.1140/epjc/s10052-023-11333-0

THE EUROPEAN PHYSICAL JOURNAL C

Regular Article - Theoretical Physics

Production of X_b via $\Upsilon(5S, 6S)$ radiative decays

Xiao-Yun Wang[1], **Zu-Xin Cai**[1], **Gang Li**[1,a], **Shi-Dong Liu**[1,b], **Chun-Sheng An**[2,c], **Ju-Jun Xie**[3,4,5]

[1] School of Physics and Physical Engineering, Qufu Normal University, Qufu 273165, China
[2] School of Physical Science and Technology, Southwest University, Chongqing 400715, China
[3] Institute of Modern Physics, Chinese Academy of Sciences, Lanzhou 730000, China
[4] School of Nuclear Science and Technology, University of Chinese Academy of Sciences, Beijing 101408, China
[5] Southern Center for Nuclear-Science Theory (SCNT), Institute of Modern Physics, Chinese Academy of Sciences, Huizhou 516000, Guangdong, China

Received: 13 January 2023 / Accepted: 12 February 2023 / Published online: 1 March 2023

Abstract We investigate the production of X_b in the process $\Upsilon(5S, 6S) \to \gamma X_b$, where X_b is assumed to be a $B\bar{B}^*$ molecular state. Two kinds of meson loops of $B^{(*)}\bar{B}^{(*)}$ and $B_1'\bar{B}^{(*)}$ were considered. To explore the rescattering mechanism, we calculated the relevant branching ratios using the effective Lagrangian based on the heavy quark symmetry. The branching ratios for the $\Upsilon(5S, 6S) \to \gamma X_b$ were found to be at the orders of $10^{-7} \sim 10^{-6}$. Such sizeable branching ratios might be accessible at BelleII, which would provide important clues to the inner structures of the exotic state X_b.

1 Introduction

In the past decades, many *XYZ* states have been observed by experiments [1]. Some of them cannot be accommodated in the conventional quark model as $Q\bar{Q}$ ($Q = c$, b) and thus become excellent candidates for exotic states. In order to understand the nature of the *XYZ* states, many studies on their productions and decays have been carried out (for recent reviews, see Refs. [2–9]). In 2003, the Belle Collaboration discovered an exotic candidate $X(3872)$ (also known as $\chi_{c1}(3872)$) in $B^+ \to K^+ + J/\psi\pi^+\pi^-$ decay [10]. Subsequently, the $X(3872)$ was confirmed by several other experiments [11–15]. Its quantum numbers were determined to be $I^G(J^{PC}) = 0^+(1^{++})$ [16]. The $X(3872)$ has two salient features: the very narrow total decay width ($\Gamma_X <$ 1.2 MeV), when compared to the typical hadronic width, and the closeness of mass to the threshold of $D^0\bar{D}^{*0}$ ($M_{X(3872)} - M_{D^0} - M_{D^{*0}} = (-0.12 \pm 0.24)$ MeV) [1]. These two features suggest that the $X(3872)$ might be a $\bar{D}D^*$ molecular state [17,18].

A lot of theoretical effort has been made to understand the nature of $X(3872)$ since its initial observation. Naturally, it follows to look for the counterpart with $J^{PC} = 1^{++}$ (denoted as X_b hereafter) in the bottom sector. These two states, which are related by heavy quark symmetry, should have some universal properties. The search for X_b could provide us the discrimination between a compact multiquark configuration and a loosely bound hadronic molecule configuration. Since the mass of X_b is very heavy and its J^{PC} are 1^{++}, a direct discovery is unlikely at the current electron-positron collision facilities, though the $\Upsilon(5S, 6S)$ radiative decays are possible in the Super KEKB [19]. In Refs. [20,21], a search for X_b in the $\omega\Upsilon(1S)$ final states has been presented, but no significant signal is observed. The production of X_b at the LHC and the Tevatron [22,23] and other exotic states at hadron colliders [24–29] have been extensively investigated. In the bottomonium system, the isospin is almost perfectly conserved, which may explain the escape of X_b in the recent CMS search [30]. As a result, the radiative decays and isospin conserving decays are of high priority in searching X_b [31–34]. In Ref. [31], we have studied the radiative decays $X_b \to \gamma\Upsilon(nS)$ ($n = 1, 2, 3$), with X_b being a candidate for the $B\bar{B}^*$ molecular state, and the partial widths into γX_b were found to be about 1 keV. In this work, we revisit the X_b production in $\Upsilon(5S, 6S) \to \gamma X_b$ using the nonrelativistic effective field theory (NREFT). As is well known, the intermediate meson loop (IML) transition is one of the important nonperturbative transition mechanisms [35–37]. Moreover, the recent studies on the productions and decays of exotic states [38–48] lead to global agreement with the experimental data. Hence, to investigate the process $\Upsilon(5S, 6S) \to \gamma X_b$,

[a] e-mail: gli@qfnu.edu.cn (corresponding author)
[b] e-mail: liusd@qfnu.edu.cn
[c] e-mail: ancs@swu.edu.cn

we calculated the IML contributions from both the S- and P-wave intermediate bottomed mesons.

The rest of the paper is organized as follows. In Sec. 2, we present the theoretical framework used in this work. Then in Sec. 3 the numerical results are presented, and a brief summary is given in Sec. 4.

2 Theoretical framework

2.1 Triangle diagrams

Under the assumption that X_b is a $B\bar{B}^*$ molecule, its production can be described by the triangle diagrams in Fig. 1. With the quantum numbers of 1^{--}, the initial bottomonium can couple to either two S-wave bottomed mesons in a P-wave, or one P-wave and one S-wave bottomed mesons in an S- or D-wave. The X_b couples to the $B\bar{B}^*$ pair in an S-wave. Because the states considered here are close to the open bottomed mesons thresholds, the intermediate bottomed and antibottomed mesons in Fig. 1 are nonrelativistic. We are thus allowed to use a nonrelativistic power counting, the framework of which has been introduced to study the intermediate meson loop effects [47]. The three momentum scales as v, the kinetic energy scales as v^2, and each of the nonrelativistic propagator scales as v^{-2}. The S-wave vertices are independent of the velocity, while the P-wave vertices scale as v or as the external momentum, depending on the process in question.

Here we do a power counting analysis to illustrate that Fig. 1 has the predominant contribution of $\Upsilon(5S, 6S) \to \gamma X_b$ in our model. For the diagrams (a), (b), and (c) in Fig. 1, the vertices involving the initial bottomonium are in a P-wave. The momentum in these vertices is contracted with the final photon momentum q and thus should be counted as q. The vertices involving the photon are also in a P-wave, which should be counted as q. The decay amplitude scales as

$$\mathcal{A}_A \sim N_A \frac{v_A^5}{(v_A^2)^3} \frac{q^2}{m_B^2} = N_A \frac{E_\gamma^2}{v_A m_B^2}, \tag{1}$$

where E_γ is the external photon energy, N_A contains all the constant factors. $v_A = (v_1 + v_2)/2$ is the average of the two velocities corresponding to the two cuts in the triangle diagram. These two velocities may be estimated as $v_1 = \sqrt{|m_1 + m_2 - M_i|/\mu_{12}}$ and $v_2 = \sqrt{|m_2 + m_3 - M_f|/\mu_{23}}$, where M_i and M_f are the masses of initial bottomonium and final X_b, respectively. m_1, m_2, and m_3 represent the masses of up, down, and right bottomed mesons in the triangle loop of Fig. 1, respectively. $\mu_{ij} = m_i m_j/(m_i + m_j)$ are the reduced masses. For $\Upsilon(5S) \to \gamma X_b$ and $\Upsilon(6S) \to \gamma X_b$ of Fig. 1a–c, we obtain $v_A \simeq 0.22$-0.24 for $\Upsilon(5S) \to \gamma X_b$ and $v_A \simeq 0.26$-0.28 for $\Upsilon(6S) \to \gamma X_b$. Therefore, the amplitude is greatly enhanced from Eq. (1). While for the diagrams (d) and (e) in Fig. 1, all the vertices are in S-wave. Then the amplitude for the Fig. 1d, e scales as

$$\mathcal{A}_B \sim N_B \frac{v_B^5}{(v_B^2)^3} \frac{E_\gamma}{m_B} = N_B \frac{E_\gamma}{v_B m_B}. \tag{2}$$

Since $v_B \simeq 0.15$ for $\Upsilon(5S) \to \gamma X_b$ and $v_B \simeq 0.21$ for $\Upsilon(6S) \to \gamma X_b$, the amplitude of Fig. 1d, e is also greatly enhanced by a factor $1/v_B$.

2.2 Effective interaction Lagrangians

To calculate the diagrams in Fig. 1, we employ the effective Lagrangians constructed in the heavy quark limit. In this limit, the S-wave heavy-light mesons form a spin multiplet $H = (P, V)$ with $s_l^P = 1/2^-$, where P and V denote the pseudoscalar and vector heavy mesons, respectively, i.e., $P(V) = (B^{(*)+}, B^{(*)0}, B_s^{(*)0})$. The $s_l^P = 1/2^+$ states are collected in $S = (P_0^*, P_1')$ with P_0^* and P_1' denoting the B_0^* and B_1' states, respectively. In the two-component notation [49,50], the spin multiplets are given by

$$\begin{aligned} H_a &= \vec{V}_a \cdot \vec{\sigma} + P_a, \\ S_a &= \vec{P}'_{1a} \cdot \vec{\sigma} + P^*_{0a}, \end{aligned} \tag{3}$$

where $\vec{\sigma}$ is the Pauli matrix, and a is the light flavor index. The fields for their charge conjugated mesons are

$$\begin{aligned} \bar{H}_a &= -\vec{\bar{V}}_a \cdot \vec{\sigma} + \vec{\bar{P}}_a, \\ \bar{S}_a &= -\vec{\bar{P}}'_{1a} \cdot \vec{\sigma} + \vec{\bar{P}}^*_{0a}. \end{aligned} \tag{4}$$

Considering the parity, the charge conjugation, and the spin symmetry, the leading order Lagrangian for the coupling of the S-wave bottomonium fields to the bottomed and antibottomed mesons can be written as [49]

$$\begin{aligned} \mathcal{L}_{\Upsilon(5S)} = {} & i\frac{g_1}{2} Tr[\bar{H}_a^\dagger \vec{\sigma} \cdot \overleftrightarrow{\partial} H_a^\dagger \Upsilon] \\ & + g_2 Tr[\bar{H}_a^\dagger S_a^\dagger \Upsilon + \bar{S}_a^\dagger H_a^\dagger \Upsilon] + \text{H.c.} \end{aligned} \tag{5}$$

Here $A \overleftrightarrow{\partial} B = A(\partial B) - (\partial A)B$. The field for the S-wave Υ and η_b is $\Upsilon = \vec{\Upsilon} \cdot \vec{\sigma} + \eta_b$. g_1 and g_2 are the coupling constants of $\Upsilon(5S)$ to a pair of $1/2^-$ bottom mesons and a $1/2^-$-$1/2^+$ pair of bottom mesons, respectively. We use g_1' and g_2' for the coupling constants of $\Upsilon(6S)$. Using the experimental branching ratios and widths of $\Upsilon(5S, 6S)$ [1], we get the coupling constants $g_1 = 0.1\ \text{GeV}^{-3/2}$ and $g_1' = 0.08\ \text{GeV}^{-3/2}$. On the other hand, we take $g_2 = g_2' = 0.05\ \text{GeV}^{-1/2}$, as used in the previous work [51].

To get the transition amplitude, we also need to know the photonic coupling to the bottomed mesons. The magnetic coupling of the photon to the S-wave bottomed mesons is

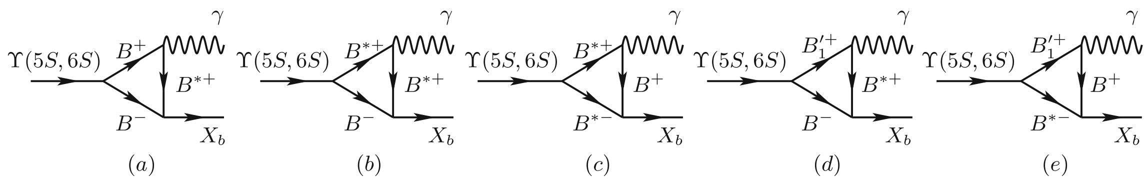

Fig. 1 Feynman diagrams for X_b production in $\Upsilon(5S, 6S) \to \gamma X_b$ under the $B\bar{B}^*$ meson loop effects

described by the Lagrangian [50,52]

$$\mathcal{L}_{HH\gamma} = \frac{e\beta}{2} Tr[H_a^\dagger H_b \vec{\sigma} \cdot \vec{B} Q_{ab}] + \frac{eQ'}{2m_Q} Tr[H_a^\dagger \vec{\sigma} \cdot \vec{B} H_a], \tag{6}$$

where $Q = \text{diag}\{2/3, -1/3, -1/3\}$ is the light quark charge matrix, and Q' is the heavy quark electric charge (in units of e). β is an effective coupling constant and, in this work, we take $\beta \simeq 3.0\ \text{GeV}^{-1}$, which is determined in the nonrelativistic constituent quark model and has been adopted in the study of radiative D^* decays [52]. In Eq. (6), the first term is the magnetic moment coupling of the light quarks, while the second one is the magnetic moment coupling of the heavy quark and hence is suppressed by $1/m_Q$. The radiative transition of the $1/2^+$ bottomed mesons to the $1/2^-$ states may be parameterized as [53]

$$\mathcal{L}_{SH\gamma} = -\frac{ie\widetilde{\beta}}{2} Tr[H_a^\dagger S_b \vec{\sigma} \cdot \vec{E} Q_{ba}], \tag{7}$$

where $\widetilde{\beta} = 0.42\ \text{GeV}^{-1}$ is the same as used in Ref. [54].

The X_b is assumed to be an S-wave molecule with $J^{PC} = 1^{++}$, which is given by the superposition of $B^0\bar{B}^{*0} + c.c$ and $B^-\bar{B}^{*+} + c.c$ hadronic configurations:

$$|X_b\rangle = \frac{1}{2}[(|B^0\bar{B}^{*0}\rangle - |B^{*0}\bar{B}^0\rangle) + (|B^+B^{*-}\rangle - |B^-B^{*+}\rangle)]. \tag{8}$$

Therefore, we can parameterize the coupling of X_b to the bottomed mesons in terms of the following Lagrangian

$$\mathcal{L} = \frac{1}{2} X^{i\dagger}[x_1(B^{*0i}\bar{B}^0 - B^0\bar{B}^{*0i}) + x_2(B^{*+i}B^- - B^+B^{*-i})] + \text{H.c.}, \tag{9}$$

where x_i denotes the coupling constant. Since the X_b is slightly below the S-wave $B\bar{B}^*$ threshold, the effective coupling of this state is related to the probability of finding the $B\bar{B}^*$ component in the physical wave function of the bound states and the binding energy, $\epsilon_{X_b} = m_B + m_{B^*} - m_{X_b}$ [40,55,56]

$$x_i^2 \equiv 16\pi(m_B + m_{B^*})^2 c_i^2 \sqrt{\frac{2\epsilon_{X_b}}{\mu}}, \tag{10}$$

where $c_i = 1/\sqrt{2}$ and $\mu = m_B m_{B^*}/(m_B + m_{B^*})$ is the reduced mass. Here, it should be pointed out that the coupling constant x_i in Eq. (10) is based on the assumption that X_b is a shallow bound state where the potential binding the mesons is short-ranged.

The decay amplitudes of the triangle diagrams in Fig. 1 can be obtained and the explicit transition amplitudes for $\Upsilon(5S, 6S) \to \gamma X_b$ are presented in Appendix A. The partial decay widths of $\Upsilon(5S, 6S) \to \gamma X_b$ are given by

$$\Gamma(\Upsilon(5S, 6S) \to \gamma X_b) = \frac{E_\gamma |\mathcal{M}_{\Upsilon(5S,6S)\to\gamma X_b}|^2}{24\pi M^2_{\Upsilon(5S,6S)}}, \tag{11}$$

where E_γ is the photon energies in the $\Upsilon(5S, 6S)$ rest frame.

In Ref. [57], authors predicted a large width of 238 MeV for B_1'. This large width effect for B_1' was taken into account in our calculations by using the Breit–Wigner parameterization to approximate the spectral function of the $1/2^+$ bottom meson of width. The explicit formula for B_1' is

$$\mathcal{M}_{B_1'} = \frac{1}{W_{B_1'}} \int_{s_l}^{s_h} \mathrm{d}s \rho_{B_1'}(s) \bar{\mathcal{M}}_{B_1'}(s), \tag{12}$$

where $W_{B_1'} = \int_{s_l}^{s_h} \mathrm{d}s \rho_{B_1'}(s)$ is the normalization factor, $\bar{\mathcal{M}}_{B_1'}(s)$ represents the loop amplitude of B_1' calculated using s as the mass squared, $s_l = (M_B + m_\gamma)^2$, $s_h = (M_{B_1'} + \Gamma_{B_1'})^2$, and $\rho_{B_1'}(s)$ is the spectral function of B_1'

$$\rho_{B_1'}(s) = \frac{1}{\pi} \text{Im} \frac{-1}{s - M^2_{B_1'} + iM_{B_1'}\Gamma_{B_1'}}. \tag{13}$$

3 Numerical results

Before proceeding to the numerical results, we first briefly review the predictions of the mass of X_b. The existence of the X_b is predicted in both the tetraquark model [58] and those involving a molecular interpretation [59–61]. In Ref. [58], the mass of the lowest-lying 1^{++} $\bar{b}\bar{q}bq$ tetraquark is predicated to be 10504 MeV, while the mass of the $B\bar{B}^*$ molecular state is predicated to be a few tens of MeV higher [59–61]. For example, in Ref. [59], the mass was predicted to be 10562 MeV, corresponding to a binding energy of 42 MeV, while with a binding energy of (24^{+8}_{-9}) MeV it was predicted to be (10580^{+9}_{-8}) MeV [61]. Therefore, it might be a good approximation and might be applicable if the binding energy is less than 50 MeV. In order to cover the range for the previous molecular and tetraquark predictions in

Table 1 The predicted decay widths (in units of keV) of $\Upsilon(5S) \to \gamma X_b$ for different binding energies. Here we choose the $\Gamma_{B_1'}$ to be 0, 100, and 200 MeV, respectively

Binding energy	$B^{(*)}\bar{B}^{(*)}$ loops	$B_1'\bar{B}^{(*)}$ loops			Total decay widths		
		$\Gamma_{B_1'}=0$	$\Gamma_{B_1'}=100$	$\Gamma_{B_1'}=200$	$\Gamma_{B_1'}=0$	$\Gamma_{B_1'}=100$	$\Gamma_{B_1'}=200$
$\epsilon_{X_b}=5$ MeV	7.24×10^{-4}	2.22×10^{-2}	1.43×10^{-3}	3.13×10^{-4}	2.77×10^{-2}	3.25×10^{-3}	1.49×10^{-3}
$\epsilon_{X_b}=10$ MeV	1.07×10^{-3}	2.01×10^{-2}	1.47×10^{-3}	3.52×10^{-4}	2.69×10^{-2}	3.87×10^{-3}	1.99×10^{-3}
$\epsilon_{X_b}=25$ MeV	1.92×10^{-3}	1.55×10^{-2}	1.41×10^{-3}	3.95×10^{-4}	2.41×10^{-2}	5.00×10^{-3}	3.05×10^{-3}
$\epsilon_{X_b}=50$ MeV	3.32×10^{-3}	1.19×10^{-2}	1.34×10^{-3}	4.30×10^{-4}	2.26×10^{-2}	6.62×10^{-3}	4.64×10^{-3}
$\epsilon_{X_b}=100$ MeV	6.80×10^{-3}	9.48×10^{-3}	1.34×10^{-3}	4.91×10^{-4}	2.49×10^{-2}	1.05×10^{-2}	8.39×10^{-3}

Refs. [58–61], we performed the calculations up to a binding energy of 100 MeV and choose several illustrative values of $\epsilon_{X_b} = (5, 10, 25, 50, 100)$ MeV for discussion.

In Table 1, we list the contributions of $\Upsilon(5S) \to \gamma X_b$ from $B^{(*)}\bar{B}^{(*)}$ loops, $B_1'\bar{B}^{(*)}$ loops, and the total contributions. For the B_1', we choose the $\Gamma_{B_1'}$ to be 0, 100 MeV and 200 MeV, respectively. It can be seen that the contributions from $B^{(*)}\bar{B}^{(*)}$ loops are about 10^{-3} keV. For the contributions from $B_1'\bar{B}^{(*)}$ loops, the partial decay widths decrease with increasing the width of B_1'. Without the width effects of B_1', i.e., $\Gamma_{B'} = 0$, the contributions from $B_1'\bar{B}^{(*)}$ loops are about 10^{-2} keV, while with $\Gamma_{B_1'} = 200$ MeV the contributions are about two orders of magnitude smaller. As seen, the total decay widths also decrease with increasing the width of B_1'. The obtained partial widths range from 10^{-3} to 10^{-2} keV, indicating a sizeable branching fraction from about 10^{-7} to 10^{-6}.

The results for $\Upsilon(6S) \to \gamma X_b$ are summarized in Table 2. The contributions from $B^{(*)}\bar{B}^{(*)}$ loops are about 10^{-3} keV. Different from the case of $\Upsilon(5S) \to \gamma X_b$, the contribution from $B_1'\bar{B}^{(*)}$ loops for $\Upsilon(6S) \to \gamma X_b$ is not monotonous with the width of B_1'. This finding indicate that the B_1' width has a smaller effect in $\Upsilon(6S) \to \gamma X_b$ than in $\Upsilon(5S) \to \gamma X_b$, which may be due to the fact that the mass of $\Upsilon(5S)$ is closer to the threshold of $B_1'\bar{B}^{(*)}$ than $\Upsilon(6S)$. It can be seen that the contributions from $B_1'\bar{B}^{(*)}$ loops range from 10^{-4} to 10^{-3} keV, which is about 1 order of magnitude smaller than $\Upsilon(5S)$. The total decay widths increase with increasing the width of B_1'. Similar to the case of the process $\Upsilon(5S) \to \gamma X_b$ the obtained partial widths for $\Upsilon(6S) \to \gamma X_b$ are also about 10^{-3} to 10^{-2} keV, thereby corresponding to a branching fraction of about 10^{-7}.

In Fig. 2a, we plot the decay widths and the branching ratios of $\Upsilon(5S) \to \gamma X_b$ as a function of the binding energy with $\Gamma_{B_1'} = 0$ MeV (solid line), $\Gamma_{B_1'} = 100$ MeV (dash line), and $\Gamma_{B_1'} = 200$ MeV (dotted line). The coupling constants of X_b in Eq. (10) and the threshold effects can simultaneously influence the binding energy dependence of the partial widths. With increasing the binding energy ϵ_{X_b}, the coupling strength of X_b increases, and the threshold effects decrease. Both the coupling strength of X_b and the threshold effects vary quickly in the small ϵ_{X_b} region and slowly in the large ϵ_{X_b} region. As a result, the partial width is relatively sensitive to the small ϵ_{X_b}, while at the large ϵ_{X_b} region it keeps nearly constant. As seen, at the same binding energy, the partial widths with small $\Gamma_{B_1'}$ are larger than those with large $\Gamma_{B_1'}$

In Fig. 2b, the dependences of the decay widths and the branching ratios for $\Upsilon(6S) \to \gamma X_b$ on the binding energy are shown. Similar to the case of $\Upsilon(5S) \to \gamma X_b$, the partial width is relatively sensitive to the small ϵ_{X_b}, while at the large ϵ_{X_b} region, it becomes nearly independent of the binding energy. As shown in this figure, at the same binding energy, the partial widths increases with the increase of $\Gamma_{B_1'}$. It can be seen that the predicted partial width for $\Upsilon(6S) \to \gamma X_b$ is insensitive to the B_1' width, which is different from the case of $\Upsilon(5S) \to \gamma X_b$. This indicates that the intermediate bottomed meson loop contribution to the process $\Upsilon(6S) \to \gamma X_b$ is smaller than that to $\Upsilon(5S) \to \gamma X_b$.

4 Summary

We have presented the production of X_b in the radiative decays of $\Upsilon(5S, 6S)$. The X_b is assumed to be a molecular state of $B\bar{B}^*$. The numerical calculations were performed under two kinds of intermediate bottomed meson loops. The first kind is $B^{(*)}\bar{B}^{(*)}$ loop coupled with $\Upsilon(5S, 6S)$ in P-wave and the second is $B_1'\bar{B}^{(*)}$ loop coupled with $\Upsilon(5S, 6S)$ in S-wave. Our results show that the partial widths of $\Upsilon(5S, 6S) \to \gamma X_b$ range from 10^{-3} to 10^{-2} keV, which correspond to the branching ratios from 10^{-7} to 10^{-6}. In Refs. [31,32], we have studied the radiative decays and the hidden bottomonium decays of X_b. If we consider that the branching ratios of the isospin conserving process $X_b \to \omega\Upsilon(1S)$ are relatively large, a search for $\Upsilon(5S) \to \gamma X_b \to \gamma\omega\Upsilon(1S)$ may be possible for the updated BelleII experiments. These studies may help us investigate the X_b deeply. The experimental observation of X_b will provide us further insight into the spectroscopy of exotic states and is helpful

Table 2 The predicted decay widths (in units of keV) of $\Upsilon(6S) \to \gamma X_b$ for different binding energies. Here we choose the $\Gamma_{B_1'}$ to be 0, 100, and 200 MeV, respectively

Binding energy	$B^{(*)}\bar{B}^{(*)}$ loops	$B_1'\bar{B}^{(*)}$ loops			Total decay widths		
		$\Gamma_{B_1'}=0$	$\Gamma_{B_1'}=100$	$\Gamma_{B_1'}=200$	$\Gamma_{B_1'}=0$	$\Gamma_{B_1'}=100$	$\Gamma_{B_1'}=200$
$\epsilon_{X_b}=5$ MeV	1.52×10^{-3}	5.67×10^{-4}	1.11×10^{-3}	4.15×10^{-4}	8.19×10^{-4}	1.10×10^{-3}	1.50×10^{-3}
$\epsilon_{X_b}=10$ MeV	2.22×10^{-3}	7.52×10^{-4}	1.27×10^{-3}	5.11×10^{-4}	1.25×10^{-3}	1.62×10^{-3}	2.20×10^{-3}
$\epsilon_{X_b}=25$ MeV	3.87×10^{-3}	1.01×10^{-3}	1.41×10^{-3}	6.38×10^{-4}	2.40×10^{-3}	2.90×10^{-3}	3.80×10^{-3}
$\epsilon_{X_b}=50$ MeV	6.39×10^{-3}	1.17×10^{-3}	1.45×10^{-3}	7.27×10^{-4}	4.39×10^{-3}	4.99×10^{-3}	6.19×10^{-3}
$\epsilon_{X_b}=100$ MeV	1.21×10^{-2}	1.27×10^{-3}	1.46×10^{-3}	8.22×10^{-4}	9.24×10^{-3}	9.77×10^{-3}	1.15×10^{-2}

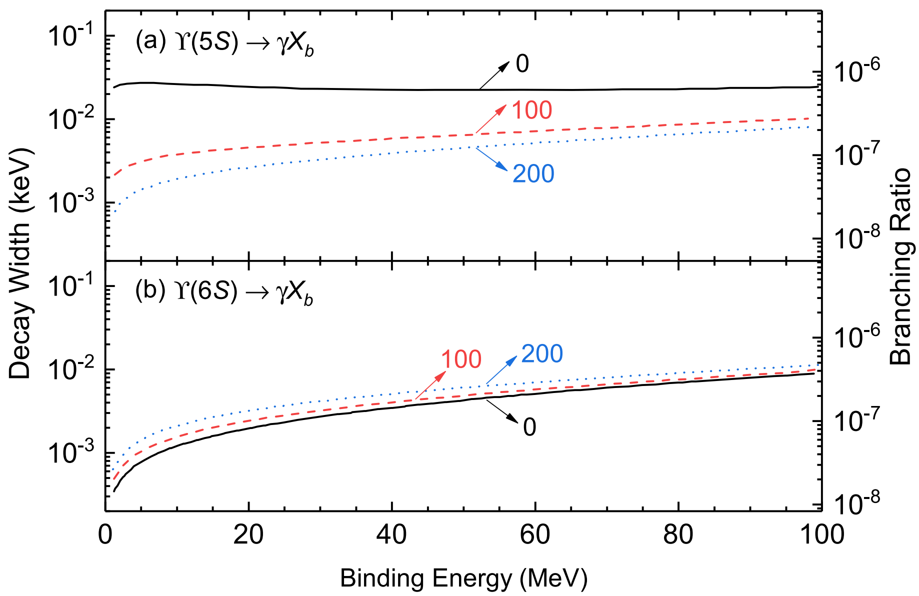

Fig. 2 The dependence of the decay widths of $\Upsilon(5S) \to \gamma X_b$ (a) and $\Upsilon(6S) \to \gamma X_b$ (b) on the binding energy for different B_1' widths as indicated by the numbers in the graph. The right y-axis represents the corresponding branching ratio

to probe the structure of the states connected by the heavy quark symmetry.

Acknowledgements This work is partly supported by the National Natural Science Foundation of China under Grant Nos. 12075133, 12105153, 12075288, 11735003, 11961141012, and 11835015, and by the Natural Science Foundation of Shandong Province under Grant Nos. ZR2021MA082, and ZR2022ZD26. It is also supported by Taishan Scholar Project of Shandong Province (Grant No.tsqn202103062), the Higher Educational Youth Innovation Science and Technology Program Shandong Province (Grant No. 2020KJJ004), the Chongqing Natural Science Foundation under Project No. cstc2021jcyj-msxmX0078, and the Youth Innovation Promotion Association CAS.

Data Availability Statement This manuscript has no associated data or the data will not be deposited. [Authors' comment: All the relevant data are already contained in the manuscript.]

Funded by SCOAP[3]. SCOAP[3] supports the goals of the International Year of Basic Sciences for Sustainable Development.

Appendix A: The transition amplitudes

Here we give the amplitudes for the transitions $\Upsilon(5S, 6S) \to \gamma X_b$. ϵ_1, ϵ_2, and ϵ_3 are the polarization vectors of the initial state $\Upsilon(5S, 6S)$, final photon γ, and final state X_b, respectively. The transition amplitudes shown in Fig. 1a–c are

$$\mathcal{M}_a = -eg_1g_X\left(\beta Q + \frac{Q'}{m_Q}\right) \times\epsilon_{ijk}q^i\epsilon_2^j\epsilon_3^k\epsilon_1\cdot q I_a^{(1)}(m_B, m_B, m_{B^*}, q), \tag{A1}$$

$$\mathcal{M}_b = eg_1g_X\left(\beta Q - \frac{Q'}{m_Q}\right) \times\epsilon_{ijk}\epsilon_1^i q^j(q\cdot\epsilon_3\epsilon_2^k - q^k\epsilon_2\cdot\epsilon_3) I_b^{(1)}(m_{B^*}, m_B, m_{B^*}, q), \tag{A2}$$

$$\mathcal{M}_c = -eg_1g_X\left(\beta Q + \frac{Q'}{m_Q}\right)\epsilon_{ijk}q^i\epsilon_2^j \times\left(\epsilon_1^k q\cdot\epsilon_3 - q\cdot\epsilon_1\epsilon_3^k + q^k\epsilon_1\cdot\epsilon_3\right) I_c^{(1)}(m_{B^*}, m_{B^*}, m_B, q). \tag{A3}$$

The transition amplitudes shown in Fig. 1d, e are

$$\mathcal{M}_d = eQ\widetilde{\beta}g_2g_X\epsilon^{ijk}\epsilon_1^i\epsilon_2^j\epsilon_3^k E_\gamma I(m_{B_1'}, m_B, m_{B^*}, q), \tag{A4}$$

$$\mathcal{M}_e = -eQ\widetilde{\beta}g_2g_X\epsilon^{ijk}\epsilon_1^i\epsilon_2^j\epsilon_3^k E_\gamma I(m_{B_1'}, m_{B^*}, m_B, q). \tag{A5}$$

In the above amplitudes, the basic three-point loop function $I(q)$ is [47]

$$\begin{aligned} &I(m_1, m_2, m_3, q)\\ &= i\int\frac{d^dl}{(2\pi)^d}\frac{1}{(l^2-m_1^2+i\epsilon)[(P-l)^2-m_2^2+i\epsilon][(l-q)^2-m_3^2]+i\epsilon}\\ &= \frac{\mu_{12}\mu_{23}}{16\pi m_1m_2m_3}\frac{1}{\sqrt{a}}\left(\tan^{-1}\left(\frac{c'-c}{2\sqrt{ac}}\right)\right.\\ &\quad\left.+\tan^{-1}\left(\frac{2a+c'-c}{2\sqrt{a(c'-a)}}\right)\right). \end{aligned} \tag{A6}$$

Here $\mu_{ij} = m_im_j/(m_i+m_j)$ are the reduced masses, $b_{12} = m_1+m_2-M$, $b_{23} = m_2+m_3+q^0-M$, and M represents the mass of the initial particle. $a = (\mu_{23}/m_3)^2\,\vec{q}^{\,2}$, $c = 2\mu_{12}b_{12}$, and $c' = 2\mu_{23}b_{23} + \mu_{23}\vec{q}^{\,2}/m_3$. m_1, m_2, and m_3 represent the masses of up, down, and right bottomed mesons in the triangle loop, respectively.

The involved vector loop integral is defined as

$$\begin{aligned} &q^iI^{(1)}(m_1, m_2, m_3, q)\\ &= i\int\frac{d^dl}{(2\pi)^d}\frac{l^i}{(l^2-m_1^2+i\epsilon)[(P-l)^2-m_2^2+i\epsilon][(l-q)^2-m_3^2]+i\epsilon}. \end{aligned} \tag{A7}$$

Using the technique of tensor reduction, we get

$$I^{(1)}(m_1, m_2, m_3, q) \simeq \frac{\mu_{23}}{am_3}\left[B(c'-a) - B(c) + \frac{1}{2}(c'-c)I(m_1, m_2, m_3, q)\right], \tag{A8}$$

where the function $B(c)$ is

$$B(c) = -\frac{\mu_{12}\mu_{23}}{4m_1m_2m_3}\frac{\sqrt{c-i\epsilon}}{4\pi}. \tag{A9}$$

It is worth mentioning that a factor $\sqrt{M_iM_f}m_1m_2m_3$ should be multiplied in each amplitude, when considering the nonrelativistic normalization of the bottomonium and bottomed meson fields, where M_i and M_f represent the masses of the initial and final particles, respectively.

References

1. R.L. Workman et al. [Particle Data Group], PTEP **2022**, 083C01 (2022). https://doi.org/10.1093/ptep/ptac097
2. H.X. Chen, W. Chen, X. Liu, S.L. Zhu, Phys. Rep. **639**, 1–121 (2016). arXiv:1601.02092 [hep-ph]
3. H.X. Chen, W. Chen, X. Liu, Y.R. Liu, S.L. Zhu, Rep. Prog. Phys. **80**, 076201 (2017). arXiv:1609.08928 [hep-ph]
4. A. Esposito, A. Pilloni, A.D. Polosa, Phys. Rep. **668**, 1–97 (2017). arXiv:1611.07920 [hep-ph]
5. F.K. Guo, C. Hanhart, U.G. Meißner, Q. Wang, Q. Zhao, B.S. Zou, Rev. Mod. Phys. **90**, 015004 (2018). arXiv:1705.00141 [hep-ph]
6. S.L. Olsen, T. Skwarnicki, D. Zieminska, Rev. Mod. Phys. **90**, 015003 (2018). arXiv:1708.04012 [hep-ph]
7. Y.R. Liu, H.X. Chen, W. Chen, X. Liu, S.L. Zhu, Prog. Part. Nucl. Phys. **107**, 237–320 (2019). arXiv:1903.11976 [hep-ph]
8. N. Brambilla, S. Eidelman, C. Hanhart, A. Nefediev, C.P. Shen, C.E. Thomas, A. Vairo, C.Z. Yuan, Phys. Rep. **873**, 1–154 (2020). arXiv:1907.07583 [hep-ex]
9. F.K. Guo, X.H. Liu, S. Sakai, Prog. Part. Nucl. Phys. **112**, 103757 (2020). arXiv:1912.07030 [hep-ph]
10. S.K. Choi et al. [Belle Collaboration], Phys. Rev. Lett. **91**, 262001 (2003). arXiv:hep-ex/0309032
11. B. Aubert et al. [BaBar Collaboration], Phys. Rev. D **71**, 071103 (2005). arXiv:hep-ex/0406022
12. V.M. Abazov et al. [D0 Collaboration], Phys. Rev. Lett. **93**, 162002 (2004). arXiv:hep-ex/0405004
13. T. Aaltonen et al. [CDF Collaboration], Phys. Rev. Lett. **103**, 152001 (2009). arXiv:0906.5218 [hep-ex]
14. S. Chatrchyan et al. [CMS Collaboration], JHEP **1304**, 154 (2013). arXiv:1302.3968 [hep-ex]
15. R. Aaij et al. [LHCb Collaboration], Phys. Rev. Lett. **110**(22), 222001 (2013). arXiv:1302.6269 [hep-ex]
16. R. Aaij et al. [LHCb], Phys. Rev. D **92**(1), 011102 (2015). https://doi.org/10.1103/PhysRevD.92.011102. arXiv:1504.06339 [hep-ex]
17. N.A. Tornqvist, Phys. Lett. B **590**, 209 (2004). arXiv:hep-ph/0402237
18. C. Hanhart, Y.S. Kalashnikova, A.E. Kudryavtsev, A.V. Nefediev, Phys. Rev. D **76**, 034007 (2007). arXiv:0704.0605 [hep-ph]
19. T. Aushev, W. Bartel, A. Bondar, J. Brodzicka, T.E. Browder, P. Chang, Y. Chao, K.F. Chen et al., arXiv:1002.5012 [hep-ex]
20. X.H. He et al. [Belle Collaboration], Phys. Rev. Lett. **113**(14), 142001 (2014). arXiv:1408.0504 [hep-ex]
21. I. Adachi et al. [Belle-II], arXiv:2208.13189 [hep-ex]
22. F.K. Guo, U.G. Meißner, W. Wang, Z. Yang, Eur. Phys. J. C **74**(9), 3063 (2014). arXiv:1402.6236 [hep-ph]
23. F.-K. Guo, U.-G. Meißner, W. Wang, Commun. Theor. Phys. **61**, 354 (2014). arXiv:1308.0193 [hep-ph]
24. C. Bignamini, B. Grinstein, F. Piccinini, A.D. Polosa, C. Sabelli, Phys. Rev. Lett. **103**, 162001 (2009). arXiv:0906.0882 [hep-ph]
25. A. Esposito, F. Piccinini, A. Pilloni, A.D. Polosa, J. Mod. Phys. **4**, 1569 (2013). arXiv:1305.0527 [hep-ph]
26. P. Artoisenet, E. Braaten, Phys. Rev. D **81**, 114018 (2010). arXiv:0911.2016 [hep-ph]
27. P. Artoisenet, E. Braaten, Phys. Rev. D **83**, 014019 (2011). arXiv:1007.2868 [hep-ph]
28. A. Ali, W. Wang, Phys. Rev. Lett. **106**, 192001 (2011). arXiv:1103.4587 [hep-ph]
29. A. Ali, C. Hambrock, W. Wang, Phys. Rev. D **88**, 054026 (2013). arXiv:1306.4470 [hep-ph]
30. S. Chatrchyan et al. [CMS Collaboration], Phys. Lett. B **727**, 57 (2013). arXiv:1309.0250 [hep-ex]
31. G. Li, W. Wang, Phys. Lett. B **733**, 100 (2014). arXiv:1402.6463 [hep-ph]

32. G. Li, Z. Zhou, Phys. Rev. D **91**(3), 034020 (2015). arXiv:1502.02936 [hep-ph]
33. M. Karliner, EPJ Web Conf. **71**, 00065 (2014). arXiv:1401.4058 [hep-ph]
34. Q. Wu, G. Li, F. Shao, Q. Wang, R. Wang, Y. Zhang, Y. Zheng, Adv. High Energy Phys. **2016**, 3729050 (2016). arXiv:1606.05118 [hep-ph]
35. H.J. Lipkin, Nucl. Phys. B **291**, 720 (1987)
36. H.J. Lipkin, S.F. Tuan, Phys. Lett. B **206**, 349 (1988)
37. P. Moxhay, Phys. Rev. D **39**, 3497 (1989)
38. Q. Wang, C. Hanhart, Q. Zhao, Phys. Rev. Lett. **111**, 132003 (2013). arXiv:1303.6355 [hep-ph]
39. X.-H. Liu, G. Li, Phys. Rev. D **88**, 014013 (2013). arXiv:1306.1384 [hep-ph]
40. F.-K. Guo, C. Hanhart, U.-G. Meißner, Q. Wang, Q. Zhao, Phys. Lett. B **725**, 127 (2013). arXiv:1306.3096 [hep-ph]
41. M. Cleven, Q. Wang, F.-K. Guo, C. Hanhart, U.-G. Meißner, Q. Zhao, Phys. Rev. D **87**(7), 074006 (2013). arXiv:1301.6461 [hep-ph]
42. D.-Y. Chen, X. Liu, Phys. Rev. D **84**, 094003 (2011). arXiv:1106.3798 [hep-ph]
43. G. Li, Q. Zhao, Phys. Lett. B **670**, 55–60 (2008). arXiv:0709.4639 [hep-ph]
44. G. Li, F.-L. Shao, C.-W. Zhao, Q. Zhao, Phys. Rev. D **87**(3), 034020 (2013). arXiv:1212.3784 [hep-ph]
45. G. Li, Eur. Phys. J. C **73**(11), 2621 (2013). arXiv:1304.4458 [hep-ph]
46. A.E. Bondar, A. Garmash, A.I. Milstein, R. Mizuk, M.B. Voloshin, Phys. Rev. D **84**, 054010 (2011). arXiv:1105.4473 [hep-ph]
47. F.-K. Guo, C. Hanhart, G. Li, U.-G. Meißner, Q. Zhao, Phys. Rev. D **83**, 034013 (2011). arXiv:1008.3632 [hep-ph]
48. D.-Y. Chen, X. Liu, T. Matsuki, arXiv:1208.2411 [hep-ph]
49. R. Casalbuoni, A. Deandrea, N. Di Bartolomeo, R. Gatto, F. Feruglio, G. Nardulli, Phys. Rep. **281**, 145 (1997). arXiv:hep-ph/9605342
50. J. Hu, T. Mehen, Phys. Rev. D **73**, 054003 (2006). arXiv:hep-ph/0511321
51. Q. Wu, D.Y. Chen, F.K. Guo, Phys. Rev. D **99**(3), 034022 (2019). arXiv:1810.09696 [hep-ph]
52. J.F. Amundson, C.G. Boyd, E.E. Jenkins, M.E. Luke, A.V. Manohar, J.L. Rosner, M.J. Savage, M.B. Wise, Phys. Lett. B **296**, 415 (1992). arXiv:hep-ph/9209241
53. P. Colangelo, F. De Fazio, G. Nardulli, Phys. Lett. B **316**, 555–560 (1993). arXiv:hep-ph/9307330 [hep-ph]
54. T. Mehen, R.P. Springer, Phys. Rev. D **70**, 074014 (2004). arXiv:hep-ph/0407181
55. S. Weinberg, Phys. Rev. **137**, B672 (1965)
56. V. Baru, J. Haidenbauer, C. Hanhart, Y. Kalashnikova, A.E. Kudryavtsev, Phys. Lett. B **586**, 53 (2004). arXiv:hep-ph/0308129
57. M.L. Du, M. Albaladejo, P. Fernández-Soler, F.K. Guo, C. Hanhart, U.G. Meißner, J. Nieves, D.L. Yao, Phys. Rev. D **98**(9), 094018 (2018). arXiv:1712.07957 [hep-ph]
58. A. Ali, C. Hambrock, I. Ahmed, M.J. Aslam, Phys. Lett. B **684**, 28 (2010). arXiv:0911.2787 [hep-ph]
59. N.A. Tornqvist, Z. Phys. C **61**, 525 (1994). arXiv:hep-ph/9310247
60. M. Karliner, S. Nussinov, JHEP **1307**, 153 (2013). arXiv:1304.0345 [hep-ph]
61. F.-K. Guo, C. Hidalgo-Duque, J. Nieves, M.P. Valderrama, Phys. Rev. D **88**, 054007 (2013). arXiv:1303.6608 [hep-ph]